AUTHOR(S): YOUSAF, A.B., IMRAN, M., KASAK, P., ZAVAHIR, F.S., ZAIDI, S.J. and FERNANDEZ, C.

TITLE: Enhanced and durable electrocatalytic performance of thin layer PtRu bimetallic alloys on Pd-nanocubes for methanol oxidation reactions.

YEAR: 2017

Publisher citation: YOUSAF, A.B., IMRAN, M., KASAK, P., ZAVAHIR, F.S., ZAIDI, S.J. and FERNANDEZ, C. 2017. Enhanced and durable electrocatalytic performance of thin layer PtRu bimetallic alloys on Pd-nanocubes for methanol oxidation reactions. Catalysis science and technology [online], 7(15), pages 3283-3290. Available from: https://doi.org/10.1039/c7cy00923b

OpenAIR citation: YOUSAF, A.B., IMRAN, M., KASAK, P., ZAVAHIR, F.S., ZAIDI, S.J. and FERNANDEZ, C. 2017. Enhanced and durable electrocatalytic performance of thin layer PtRu bimetallic alloys on Pd-nanocubes for methanol oxidation reactions. Catalysis science and technology, 7(15), pages 3283-3290. Held on OpenAIR [online]. Available from: https://openair.rgu.ac.uk

Catalysis Science & Technology

PAPER

View Article Online
View Journal

Cite this: DOI: 10.1039/c7cy00923b

Enhanced and durable electrocatalytic performance of thin layer PtRu bimetallic alloys on Pd-nanocubes for methanol oxidation reactions†

Ammar Bin Yousaf, *[ab] M. Imran,[b] Peter Kasak,[a] Fathima Sifani Zavahir,[a] Syed Javaid Zaidi[a] and Carlos Fernandez[c]

As a renewable and promising energy devices, direct methanol fuel cells (DMFCs) have attracted a wide range of interest in recent years. The design of electrocatalysts highly influences the performance of DMFCs systems. Herein, PtRu bimetallic alloy nanoparticles have been fabricated onto a Pd nanocube (NC) core material by a facile wet chemical co-precipitation method. Structural and morphological characterization of the catalyst was performed using X-ray photoelectron spectroscopy (XPS) analysis, energy-dispersive X-ray (EDX) spectroscopy, transmission electron microscopy (TEM), high resolution transmission electron microscopy (HRTEM), high-angle annular dark-field scanning TEM (HAADF-STEM) elemental mapping and temperature programmed reduction (TPR). The presence of a single TPR peak strongly supported bimetallic Pt–Ru interactions and alloying. The electrocatalytic performance of the as-synthesized PtRu@Pd-NC catalyst for the methanol oxidation reaction (MOR) is studied in $HClO_4$ aqueous solution by cyclic voltammetry (CV), chronoamperometry (CA) and electrochemical impedance spectroscopy (EIS), and it is compared with that of a PtRu/C (E-TEK) catalyst. The catalyst has shown the highest specific activity (*ca.* 11.44 mA cm^{-2} at 0.70 V), a lower onset potential and enhanced durability for MOR, which is significantly higher than the commercial PtRu/C (E-TEK) catalyst and other reported Pt/Pd-based catalysts. The results attribute to mutual interactions of the core–shell material that enhance the chemisorption of methanol.

Received 9th May 2017,
Accepted 19th June 2017

DOI: 10.1039/c7cy00923b

rsc.li/catalysis

Introduction

Direct methanol fuel cells (DMFCs) have been considered as some of the most promising power sources for portable electronics due to the high energy density of methanol.[1] However, the slow kinetics of the methanol oxidation reaction (MOR) at anode electrocatalysts remains one of the serious challenges which hinders the large scale commercialization of the DMFC technology. Pt materials exhibit facile adsorption and decomposition of methanol on their surfaces.[2] The strong binding of CO molecules on the Pt surfaces, which block active sites necessary for the electro-oxidation of CH_3OH, is the major origin of the sluggish kinetics of MOR.[3] Addition of Ru onto Pt electrocatalysts is found to facilitate CO oxidation through both bi-functional and ligand effects.[4] However, the scarcity and high cost of both Pt and Ru call for further efforts to develop new catalysts with ultralow precious metal loadings and improved MOR activity. Developing core–shell nanocatalysts with a second or third cheap metal as the core is also a convenient way to achieve the aims stated above.[5–8]

Over the past few decades, bimetallic alloys with Pt have attracted much attention as compared to monometallic Pt anodes and several studies have been devoted to this field due to the fact that electronic effects and metal interactions enhance electrocatalytic activity and CO tolerance in MOR studies.[9] Cost effective, tunable bi or tri-metallic composites with enhanced electrocatalytic performance are the major research highlight for present day fuel cells.[10,11] It is evident from the literature that composites of Pt with other transition elements have shown remarkably high performance and this strategy significantly overcomes the existing problems in DMFCs.[12–16] Poh *et al.*[17] developed a series of Pt-based bimetallic and trimetallic catalysts in combination with transition metals; in their approach, they claimed the enhancement of

[a] *Center for Advanced Materials, Qatar University, Doha 2713, Qatar. E-mail: muhammad.ammar@qu.edu.qa, ammar.chemist18@gmail.com*
[b] *Hefei National Laboratory for Physical Sciences at Microscale, School of Chemistry and Materials Sciences, University of Science and Technology of China, Hefei 230026, P.R. China. E-mail: ammar@mail.ustc.edu.cn*
[c] *School of Pharmacy and Life Sciences, Sir Ian Wood Building, Robert Gordon University, AB107GJ Aberdeen, UK*

† Electronic supplementary information (ESI) available: Additional physical characterization and electrochemical experimental data. See DOI: 10.1039/c7cy00923b

MOR performance facilitated *via* ligand interactions with Pt particles. Later on, Farias *et al.*[18] worked on a CO poisoning issue suffered by DMFCs; they precisely investigated that incorporation of Ru or Sn entities favorably reduced the poisoning issue by CO_{ads} species during methanol electro-oxidation. As the electrocatalytic performance of metal alloys depends largely on size and composition, an accurate intrinsic correlation of alloy metal composition is required with preferably facile synthesis routes to overcome the challenges of complex synthesis processes.[19–22] All reported physical or wet chemical methods have failed to precisely control the composition and size of alloys; therefore programmatic trials are still required to achieve a desirable state.[23]

Palladium-based materials have been widely examined as electrocatalysts for the oxidation of small organic fuels due to similar properties of Pd to those of platinum.[24] Notable enhancement in MOR activity has been reported for various binary nanomaterials such as PdPt, PdRu, PdSn, PdAu and PdMo.[25,26] Among these, Liu *et al.*[27] reported the bimetallic combination of Pd with a single nickel transition metal, and Zhao *et al.*[28] demonstrated methanol electro-oxidation on a Pd-based trimetallic combination with Pt and Cu. In addition, Yan's[29] group reported multimetallic Pd-based electrocatalysts comprising a choice of Pd and Pt with different ternary metals. All these groups concluded that introducing a binary candidate with Pd enhances the performance of a material *via* the so called bi-functional mechanism. Whereas, by combining a ternary metal with Pd, the Pd bimetallic system may remarkably improve the MOR process by several factors. Recently, materials with a preferential (100) orientation have been confirmed to have significantly higher activities toward the oxidation of small organic fuels. Due to the preferential presence of the (100) crystallographic plane and their beneficial electronic structure, it is expected that Pd nanocube (NC)-supported PtRu nano-materials may exhibit enhanced MOR activity at a significantly lower PtRu loading as compared to better MOR electrocatalysts. However, such a strategy has not been well investigated.[29–35] In this work, we will demonstrate that PtRu co-deposited onto Pd NCs with a well-defined shape (fcc 100) displays very good MOR activity.

Experimental

Reagents

K_2PdCl_4 (99.9% metal basis, from Alfa Aesar), K_2PtCl_6 (40% from Fluka), $RuCl_3$ (40% from Fluka), hexadecyltrimethylammonium bromide ($C_{16}TAB$), ascorbic acid, $HClO_4$ (from Sigma Aldrich) and CH_3OH (99.9% from J. T. Baker). All reagents were used as received without further purification.

Characterization

The crystallographic structure, morphology and atomic composition of the synthesized catalyst were studied by transmission electron microscopy (TEM), high resolution transmission electron microscopy (HRTEM), energy-dispersive X-ray spectroscopy (EDX), and X-ray photoelectron spectroscopy (XPS). The measurements were carried out using a SPeCS system (PHOIBOS 150, Germany) with AlK_α radiation ($h\nu$ = 1486.6 eV) and temperature-programmed reduction (TPR) studies were performed using an instrument named McNicol.

Synthesis of the PtRu@Pd-NC composite

The procedure for the synthesis of Pd nanocubes is reported in detail.[36–38] In brief, 500 μL of 5 mM K_2PdCl_4 aqueous solution was added to 10 mL of 1.25×10^{-2} M $C_{16}TAB$ aqueous solution at a fixed temperature of 95 °C. After 15 minutes, 80 μL of 0.1 M ascorbic acid was gradually added to the mixed solution with $C_{16}TAB$ and K_2PdCl_4 under continuous stirring for 30 minutes. Pd NCs with a size of *ca.* 25 nm were obtained after centrifuging the solutions. The as-synthesized Pd-NCs were further used for PtRu shell deposition. 1 mg mL^{-1} Pd-NCs were dispersed in Milli-Q water, a specific amount of $C_{16}TAB$ was further added and the mixture was stirred for some time. Then specific composition of Pt : Ru precursors were added simultaneously with ratios of 3 : 1 to the reaction mixture. 40 μL of 0.1 M ascorbic acid were dropped into the reaction flask and stirred for 3 hours at 80 °C temperature. The PtRu@Pd-NC core–shell material was obtained after centrifugation of the solution.

Electrochemical measurements

Before each electrochemical experiment, a glassy carbon (GC) electrode (0.196 cm^2 geometric surface area) was first polished with alumina slurry (Al_2O_3, 0.05 mm) on a polishing cloth to obtain a mirror finish. 15 μL of 1 mg mL^{-1} PtRu@Pd-NC, Pd-NC and PtRu/C (E-TEK) suspensions in ethanol were drop-coated onto the polished electrode surface separately using a microliter syringe followed by drying in a vacuum at room temperature. Afterward, the catalyst was covered with a thin layer of Nafion (0.1 wt% in water, 5 mL) to ensure that the catalyst was tightly attached to the electrode surface during the electrochemical measurements. Voltammetry measurements were carried out with a CHI750D electrochemical workstation. The electrode prepared above was used as the working electrode. Ag/AgCl (in 3 M NaCl, aq.) and a Pt coil were used as the reference and counter electrodes, respectively. All the measurements were performed in electrochemical experiments with respect to the standard values of a reversible hydrogen electrode (RHE).

Results and discussion

The desired aim of the present study is focused on the role of Pd-NCs in enhancing the electrocatalytic activity of the PtRu bimetallic alloy in the PtRu@Pd-NC core–shell catalyst. The uniform coating of the PtRu shell on the Pd NCs was the key requirement for these studies. The transmission electron microscopy (TEM) image provided in Fig. 1-a shows clear evidence of a PtRu@Pd-NC core–shell material with a well-defined cubic shape, edges and corners. The representative TEM image of the as-synthesized PtRu@Pd-NC

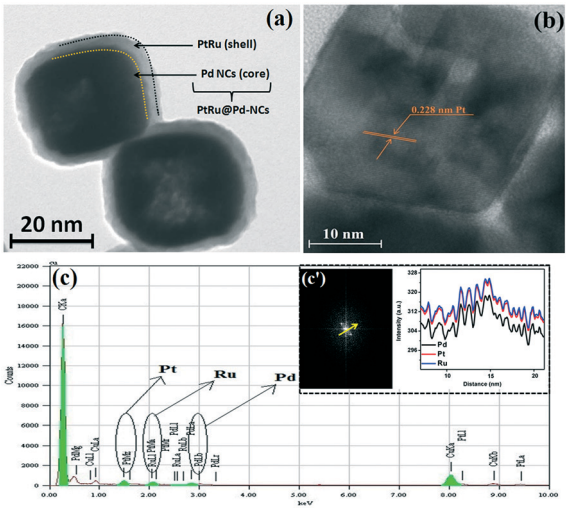

Fig. 1 (a) TEM image of the as-synthesized core–shell PtRu@Pd-NC catalyst, (b) HRTEM image of the PtRu@Pd-NC composite, and (c) corresponding EDX spectrum of PtRu@Pd-NCs (inset c′ shows the line scan spectra of the PtRu@Pd-NC core–shell catalyst obtained by HRTEM analysis).

nanocomposite exhibits an average size of 30 nm. The dark cubic region of the Pd NCs is surrounded by a light PtRu shell layer. The formation of a PtRu@Pd-NC composite has been further confirmed by HRTEM; Fig. 1-b shows the intermixed Pd lattice with Pt on the surface of the NCs exhibiting successive alloying of Pt with Pd in the composite formation. The HRTEM micrograph shows a periodicity of the lattice fringes calculated to be d = 0.227 nm, corresponding to the (111) planes of fcc Pt. From the EDX measurements (Fig. 1-c), it can be seen that the ratio of Ru, Pt and Pd in the PtRu@Pd-NC composite is 1 : 3 : 7, respectively (the small amount of carbon and copper elements came from the amorphous carbon-coated copper grids). Moreover, the line-scan spectra have also been provided to confirm the core–shell material synthesis (inset in Fig. 1-c). Furthermore, HAADF-STEM elemental mapping was performed to examine the distribution of a Pt and Ru alloy on Pd NCs. It can be clearly seen from Fig. 2 that Pt and Ru have a good dispersion, indicating the formation of a PtRu alloy uniformly coated on the surfaces of Pd-NCs. The element mapping images of a selected area, along with an overlay image, provide strong evidence for the formation of a PtRu shell over the Pd-NCs.

XPS was employed to determine the surface composition of the PtRu@Pd-NC composite (Fig. 3a–d). The full scan survey exhibited signatures of all the metals present in the composite material with intense characteristic peaks. The Ru $3p_{3/2}$ and Ru $3p_{1/2}$ peaks are centered at 464.4 eV and 487 eV, respectively, corresponding to the metallic Ru^0 states. The band assigned to Pt $4f_{7/2}$ and Pt $4f_{5/2}$ at 71.4 eV is found to be positively shifted at *ca.* 71.1 eV in comparison with that of the metallic Pt^0 state.[37] The Pt 4f peak can be further deconvoluted by using a Doniach-Sunjic line shape into two Gaussian components with a more intense doublet at binding energies of 71.4 eV and 74.6 eV, corresponding to the metallic Pt^0 state. Fig. 3(b) also shows the high resolution XPS spectra of Pd $3d_{5/2}$ and $3d_{3/2}$ with binding energies at 334.4 eV and 340 eV, respectively, corresponding to metallic Pd, which is in good agreement with the TEM results. As in the case of Pt-based alloys, the electronic structure of metals slightly changes, and the same situation is observed in our PtRu@Pd-NC composite in which the Pt 4f band shifts to higher energy and the Pd 3d shifts to lower energy and there is electron transfer from Pt to Pd which enhances the electrochemical performances. In contrast, the band of Pd $3d_{5/2}$ and $Pd3d_{3/2}$ at 334.4 eV is found to be negatively shifted from the corresponding band of the metallic Pd^0 state (335 eV).[39] The spectral shift indicates that there is partial transfer of electrons from Pt to Pd atoms. The oxidation states of the elements and the alloying between them were further confirmed by TPR studies (see Fig. 4). The TPR experiments were performed with a H_2 : Ar mixture (10 : 90 molar) flowing at about 30 mL (NTP) min^{-1} at 1 atm. After 0.12 g of the catalyst sample was charged into a quartz TPR cell, gas stream was passed through the catalyst sample. When the thermal

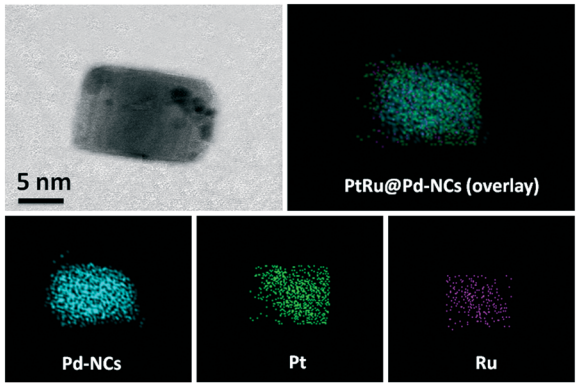

Fig. 2 HAADF-STEM elemental mapping of PtRu@Pd-NCs, PdPtRu overlay, Pd-NCs, Pt and Ru, respectively.

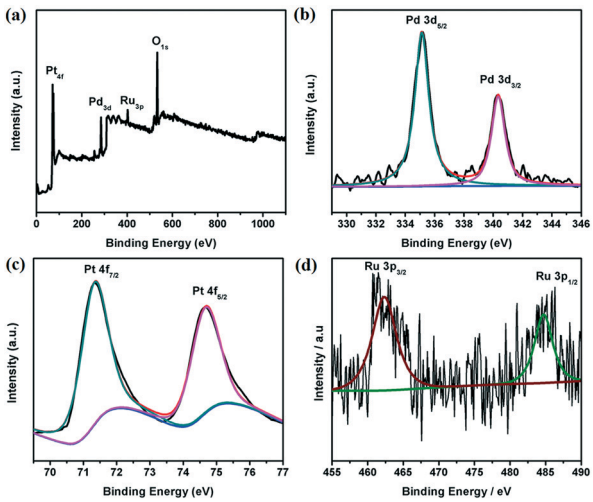

Fig. 3 (a) XPS survey scan of PtRu@Pd-NCs, (b) high resolution XPS Pd_{3d} scan, (c) high resolution XPS Pt_{4f} scan and (d) high resolution XPS Ru_{3p} scan.

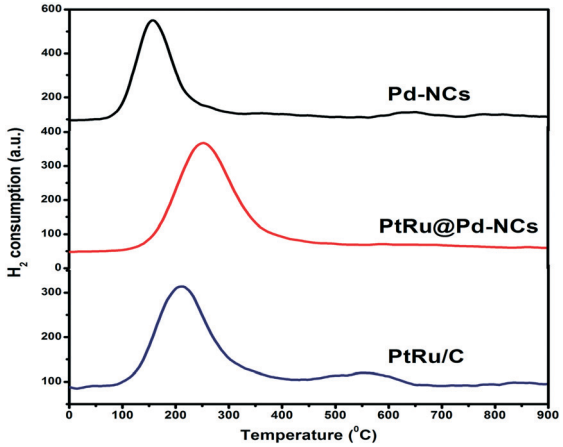

Fig. 4 Temperature-programmed reduction (TPR) spectra of Pd-NC, PtRu@Pd-NC and PtRu/C catalysts.

conductivity detector (TCD) signal became stable, the sample was heated at 10 °C min^{-1} to 900 °C using a temperature-programmed furnace. The reduction temperature was monitored with a K-type thermocouple and the water produced by reduction was trapped in a column of silica gel. The output polarity was set so that positive TCD signals indicate hydrogen consumption. The TPR spectra of PtRu@Pd-NCs exhibit a single peak, suggesting the formation of Pt–Ru bimetallic interactions and also confirming the alloying with Pd-NCs, possibly due to the close proximity of Pt and Ru in the co-reduction method.

The crystal structures of Pd NCs and PtRu@Pd-NCs were analyzed by means of X-ray diffraction (XRD) patterns. The prominent diffraction peaks are observed in Fig. 5 at 2θ = 39.90° (111), 45.50° (220) and 67.80° (220) in the case of the Pd NC XRD pattern, which are consistent with the face-centered-cubic (fcc) crystalline structure of Pd (JCPDS, card no. 46-1043). In the XRD pattern of the PtRu@Pd-NC composite, the diffraction peaks at 2θ = 39.40° (111), 46.20° (220) and 68.30° (220) correspond to Pd and Pt, respectively, while the additional peak at 2θ = 77.30° (301) clearly indicates the existence of Ru. Additional peaks of RuO_2 were not detected in the XRD spectra. In the XRD pattern of the PtRu@Pd-NC composite, the peak at (220) shifted slightly to higher angles compared to the pure Pd NCs, which indicates lattice contraction due to alloy formation, while the peak at (111) showed a shift towards lower angles corresponding to nucleation of Pt atoms on the Pd surface.

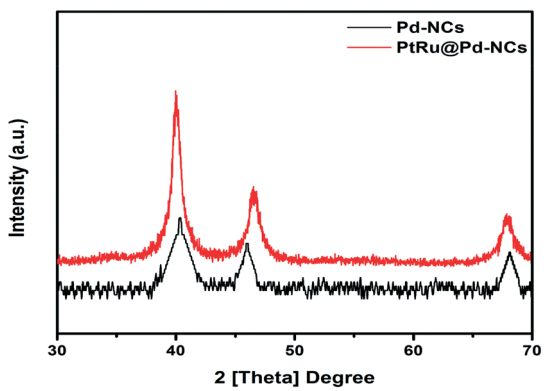

Fig. 5 X-ray diffraction spectra of Pd-NCs and PtRu@Pd-NCs.

The electrochemical performance of the as-developed PtRu@Pd-NC nanocomposite was compared with the commercial PtRu/C bimetallic alloy catalyst. In order to calculate the electrochemical active surface area (ECSA), the cyclic voltammogram (CV) curves of the catalysts were recorded from 0.05 V to 0.70 V *vs.* RHE at room temperature in N_2 purged 0.1 M $HClO_4$ aqueous solution at a scan rate of 50 mV s^{-1}. The higher anodic potential was restricted up to 0.70 V, in order to avoid the formation of ruthenium oxides and deactivation of the PtRu bimetallic alloy layer at higher potential limits. The inset in Fig. 6 and Fig. S1† show the base cyclic voltammogram (CV) for PtRu@Pd-NC and PtRu/C catalysts. The CV displays a broad current region for underpotential deposition of H (H_{UPD}) and its oxidation in the region from 0.05 to 0.35 V, similar to polycrystalline Pt. It is followed with a double layer region from 0.4 V to 0.7 V, wherein the current is slightly higher than that of pure Pt of the same surface area.

This confirms the presence of a small amount of Pt. The electrochemical surface area of the electrode composed of the PtRu@Pd-NC catalyst was determined by integrating the current for H_{UPD} and assuming the charge of H_{UPD} on smooth Pt (210 μC cm^{-2}).[40,41] In all the CVs, a characteristic current response associated with PtRu compared with the pure Pd-NC catalyst has been shown. PtRu@Pd-NCs exhibit a typical adsorption/desorption region in the CVs, which shows the hybrid alloyed structure of secondary metals with Pd, and a prominent H_{UPD} region with two peaks is also well observed. The peaks in the H_{UPD} region provide strong evidence

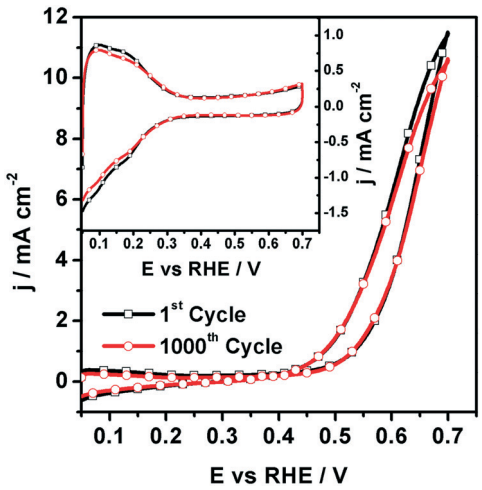

Fig. 6 The activity of methanol oxidation reaction (MOR) and the accelerated durability test in 0.1 M $HClO_4$ + 1 M CH_3OH solution at a scan rate of 50 mV s^{-1} up to 1000 cycles; the inset shows the base cyclic voltammograms before and after running MOR for 1000 cycles in the potential region from 0.05 V to 0.7 V.

of hydrogen adsorption at the (110) and (100) facets of Pt intermixed with Pd. The XPS results are also in good agreement with this electro-chemical behavior and also these H_{UPD} characteristics of our PtRu@Pd-NC catalyst are also well attributed to previously reported Pt and Pd hybrid alloys with other metals.[42–44] The electrocatalytic behaviors towards methanol electro-oxidation were measured by two electrochemical methods using CV and chronoamperometry (CA) in 0.1 M $HClO_4$ + 1 M CH_3OH solution. The cyclic voltammogram for methanol oxidation is given in Fig. 6 and Fig. S1.† Both the real current and the current densities (j) which were obtained by normalizing the current with the electrochemical active surface area (ECSA) are provided. The current densities obtained by normalizing with the geometric surface area were also measured and compared for all the catalysts (see Table S1†). The chronoamperometric current transients for MOR at constant potentials of 0.3 V, 0.4 V and 0.5 V are given in Fig. 7. The onset of the methanol oxidation reaction takes place near 0.30 V; the MOR current increases slowly with a positive shift in electrode potential up to 0.5 V, which is followed by a sharp increase at a potential from 0.5 to 0.7 V. From Fig. 7, it is demonstrated that the initial MOR current is very high. However, it drops quickly within the first 25 s. Afterwards, it drops slowly and reaches a steady state value at *ca.* 5 min after the potential step. The peak current density is 11.44 mA cm^{-2} (at 0.70 V). The obtained current density was higher than those of the commercial PtRu/C catalyst and recently reported modified catalysts with Pd-NCs. Our catalyst has shown significantly higher activity around 3 times higher than that of the commercial PtRu/C catalyst. Furthermore, the onset potential for chemisorption of methanol is at a lower potential *vs.* RHE than that of the above compared reported catalysts.

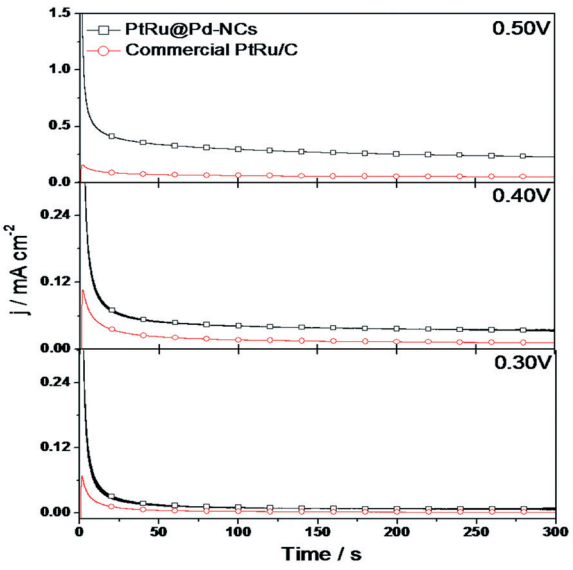

Fig. 7 Current transients of MOR for PtRu@Pd-NCs compared with commercial PtRu/C in 0.1 M $HClO_4$ + 1 M CH_3OH solution at constant potentials of 0.30 V, 0.40 V and 0.50 up to 300 s.

The enhanced MOR performance on the Pt/Pd surface may be attributed to the favorable chemisorption of methanol and subsequent breakage of the C–H bond. The removal of poisoning intermediates such as Pt–CO_{ads}/Pd–CO_{ads} by the oxidation with Pt–OH_{ads}/Pd–OH_{ads} supplied by Pt–OH/Pd–OH sites also promotes electrocatalytic activity.[45] The reported data suggest that our PtRu@Pd-NCs demonstrated much higher performance due to the promoting effect of C–H breakage and removal of CO_{ads} in the methanol electro-oxidation compared to the commercial PtRu/C. The enhanced MOR activity of PtRu@Pd-NCs can be well understood by the mechanistic explanation of chemisorption of methanol which depends on two factors; in the first factor, the Pt sites easily remove the poisoning intermediates such as CO_{ads} by the presence of OH_{ads} on nearby Ru sites and enhance methanol electro-oxidation. Secondly, the alloying of the Pt shell with the Pd core also weakens the Pt–CO_{ads} bond that may lead to the easy breakage of the Pt–CO_{ads} bond, which tends to remove poisoning intermediates and provide more Pt sites available for further electro-oxidation of methanol.

The enhanced electrocatalytic performance is also attributed to the synergistic effect provided by Pd-NCs. Our PtRu@Pd-NCs showed much higher performance than the reported materials;[46–50] this enhancement is due to the intermixing of PtRu layers with Pd-NCs, which inhibit the blockage of Pt active sites by poisoning intermediates such as CO_{ads} species. Moreover, there is a mutual electron transfer path which provides a short axial transmission distance for electrolyte ions and electrons in the electrode and thus display higher specific capacitance and transference of electrons in anodic application. There are two key parameters for a catalyst to be excellent in electro-oxidation; firstly, it should have a higher current density and secondly, it must show a lower onset oxidation potential. Our PtRu@Pd-NC catalyst exhibited the highest oxidation current/mass activity and also showed a lower onset oxidation potential.

The MOR performance of PtRu@Pd-NCs has also proved to be much better than those of other already reported Pd/Pt-based catalysts,[51] as can be seen in the critical comparison among those provided in Table 1. As the durability of electrocatalysts is one of the important issues for their applications

Table 1 Comparison of electrocatalytic MOR activity of reported Pd/Pt/Ru-based catalysts with that of our catalyst

Catalyst	j (mA cm^{-2})		Ref. no.
Pd-NCs	0.73[a]		55
Pt-NCs	1.0[a]		56
PdPt-NCs	6.0[a]		57
PtRu composite	1.90[a]		58
Pt/C commercial	0.70[a]		56
This work	11.44[a]	44.29[b]	—
Pd/TiO_x nanotubes	20[b]		59
Ru/MnO_x	7.2[b]		60

[a] Current density normalized by ECSA. [b] Current density normalized by geometric surface area at 0.70 V.

in fuel cells, an accelerated durability test (ADT) was also performed in 0.1 M $HClO_4$ + 1 M CH_3OH solution by applying a cyclic potential sweep between 0.05 V to 0.70 V *vs.* RHE at a scan rate of 100 mV s^{-1} up to 1000 cycles. The durability was tested by comparing the ECSAs from base CVs and peak currents from MOR activity before and after accelerated methanol oxidation reaction. As shown and compared with the 1st cycle of CVs in Fig. 6, the PtRu@Pd-NCs experienced a loss of only 1.3% and 1.4%, respectively, of the initial ECSA and peak current after 1000 cycles of methanol oxidation. Such results indicate that the as-synthesized PtRu@Pd-NCs exhibit enhanced durability towards methanol oxidation. This was a very significant improvement for using and tuning Pd-NCs with (100) facets by alloying with two other metals for methanol oxidation and developing a tri-metallic nanocomposite electrocatalyst as an anode material in DMFCs.

Moreover, electrochemical CO oxidation experiments were performed to strengthen the mechanistic claims in the present study (see Fig. S2†). CO is a well-known poisoning intermediate that stops further oxidation of methanol once adsorbed on the active sites of catalysts. The present study's results, it has been seen that the much higher improvement in MOR catalysis after fabricating a PtRu shell on Pd-NCs is attributed towards shifting the CO oxidation to lower potential values. As the adsorbed CO is oxidized at a lower potential, more active sites are released for oxidation of methanol molecules.

The enhanced activity and durability for MOR of PtRu@Pd-NCs compared with PtRu/C (E-TEK) bimetallic alloy NPs are suggested to be caused by the synergistic effect promoted by the Pd-NC support. This synergistic effect eventually enhanced the overall catalytic performance of the PtRu@Pd-NCs. In addition, electrochemical impedance spectroscopy (EIS) experiments were further performed to support the claim regarding the synergistic effect in the present study. The study of the electro-oxidation of methanol on PtRu@Pd-NC, Pd-NC and PtRu/C (E-TEK) electrodes was carried out with EIS measurements. The Nyquist curves of the above catalysts in the same aqueous solution for MOR studies are shown in Fig. 8. The EIS results reveal a slow reaction rate of the methanol dehydrogenation oxidation on PtRu/C (E-TEK) compared with PtRu@Pd-NCs. This suggests that the slow kinetics is caused by the CO_{ads} intermediate from methanol dehydrogenation intermediate species which are strongly adsorbed on Pt sites and block the continuous adsorption and dehydrogenation of methanol molecules.[52,53] The EIS patterns on Pd-NCs are also similar to those on the PtRu/C (E-TEK) catalyst. On the other hand, in the case of PtRu@Pd-NCs, the Nyquist curve indicates that the rate of methanol dehydrogenation is faster on this catalyst. Thus, the performance of CO-tolerance on the PtRu@Pd-NC catalyst is higher than that on the PtRu/C (E-TEK) catalyst. The EIS results suggest that the rates of electro-oxidation and removal of CO_{ads} by OH_{ads} are rapid on the PtRu@Pd-NC catalyst, thereby enhancing its catalytic activity for MOR compared to that of the PtRu/C (E-TEK) catalyst.

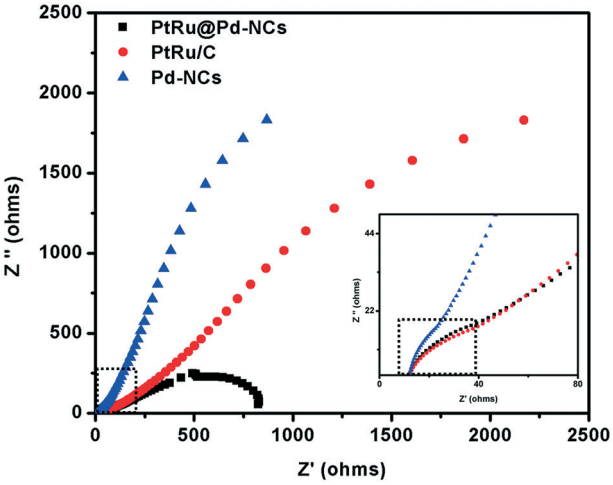

Fig. 8 Electrochemical impedance spectroscopy (EIS) Nyquist plots for PtRu@Pd-NC, PtRu/C and Pd-NC catalysts in 0.1 M $HClO_4$ + 1 M CH_3OH solution at 0.40 V *vs.* RHE, inset: the hemisphere's arc area extracted from EIS curves.

The EIS curves were also analyzed in depth to determine the impedance of each component within the system separately. The Nyquist impedance curves in the inset in Fig. 8 show two different arced areas for all the catalysts. The first arc hemisphere area possibly intercepting at the *x*-axis is ascribed to the equivalent series resistance (ESR), which is mainly associated with the resistance of electrolyte, and the effect of the catalyst is excluded here. It is clearly seen from the results that the ESR value of PtRu@Pd-NCs is comparatively lower than those of the other two catalysts provided in the present study. After the small arced hemisphere area, the data points correspond to the resistance related to the catalyst performance for chemisorption of alcohol molecules. The position of data points towards the left side indicates the successive oxidation of methanol molecules with low CO poisoning or the catalyst oxidizing CO_{ads} more effectively to allow the reaction to proceed forward.[54]

The EIS studies were further extended to analyze the resistance during MOR at different potentials (see Fig. S3†). These results also provided information about the superiority of PtRu@Pd-NC catalysts over PtRu/C (E-TEK) and the starting Pd-NC catalyst. The smooth start of methanol chemisorption seen at lower potentials showed a steady decrease with an increasing potential range up to 0.40 V in the first quadrant, the reaction proceeding with maximum oxidation of methanol. Then at 0.70 V, the adsorbed CO intermediate was removed from the active sites of the catalyst, as shown by the reverse direction of the EIS arc. This enhancement factor for the PtRu alloy in MOR is attributed to the synergistic effect of Pd-NCs. There is a possible electron transfer from the Pd-NC substrate to Pt in the PtRu shell due to the difference of electronegativity values between Pd and Pt, *i.e.* 2.20 and 2.28, respectively. The higher electronegativity of Pt compared with that of Pd suggests the electronic interactions between the Pd support and Pt atomic orbitals, leading to

transference of electrons from Pd to Pt. This electron transfer phenomenon may contribute to the decay of the Pt–CO binding energy and improve the electro-oxidation of CO_{ads}-like intermediate species from methanol dehydrogenation, and highly enhance the adsorption and oxidation of methanol molecules on the PtRu@Pd-NC catalyst.[61,62]

Our catalyst has fulfilled all the required parameters for a good anode material for DMFCs, such as having the highest activity at lower potentials, a lower onset potential and enhanced durability. The catalyst, with a lower atomic composition of PtRu along with Pd (fcc 100), has shown higher activity. This facile approach can open successive pathways to tune the present metallic support materials further, for more highly active catalysts for MOR.

Conclusions

In conclusion, we have demonstrated a novel, highly efficient and durable PtRu@Pd-NC catalyst for MOR. In our work, Pd-NCs have been used as metallic support materials to cover the PtRu bimetallic alloy shell. Material characterization has completely described the crystallographic structure and morphology of the as-developed nanocomposite. The electrochemical experimental results revealed the excellent performance of PtRu@Pd-NCs compared to the commercial PtRu/C (E-TEK) catalyst. The EIS patterns provided significant evidence of the synergistic effect of Pd-NCs on enhancing the electrocatalytic activity of PtRu bimetallic alloy NP layers on their surface.

We have been successful in achieving our goal and providing multiple contributions to the field of electrocatalysis with the present work. The most important among them is the reduced cost of catalysts with a lower composition of precious metals Pt and Ru on a Pd-based material. Hence, tuning of Pd-NCs as metallic supports for excellent MOR activity and chemical co-reduction of PtRu on Pd-NCs in order to synthesize a composite core–shell catalyst provide a better MOR catalyst with lower onset potential, higher current density at lower potentials compared to the commercial PtRu/C (E-TEK) catalyst and enhanced durability. This successful and new achievement informs us that the Pd (100) facets improve the activity in combination with low amounts of Pt and Ru metals. This study could be further adopted to produce more active and low-cost MOR catalysts with different bimetallic alloy compositions on active Pd-based materials.

Acknowledgements

The authors acknowledge financial support from the USTC fellowship programme offered by the University of Science and Technology of China and the Hefei and Anhui Government Scholarship offered by the Anhui provincial government, China. This work was also made possible by NPRP grant # 9-219-2-105 from the Qatar National Research Fund (a member of The Qatar Foundation). The findings achieved herein are solely the responsibility of the authors.

References

1 M. Shao, T. Yu, J. H. Odell, M. Jin and Y. Xia, *Chem. Commun.*, 2011, **47**, 6566–6568.
2 Z. Z. Zhu, Z. Wang and H. L. Li, *J. Power Sources*, 2009, **186**, 339–343.
3 K. Kinoshita, *J. Electrochem. Soc.*, 1990, **137**, 845–848.
4 F. Kadirgan, A. M. Kannan, T. Atilan, S. Beyhan, S. Ozenler and S. Suzer, *Int. J. Hydrogen Energy*, 2009, **34**, 4312–4316.
5 F. Kadirgan, B. Beden, J. M. Leger and C. Lamy, *J. Electroanal. Chem.*, 1981, **125**, 89–94.
6 H. A. Gasteiger, N. M. Markovic and P. N. Ross, *J. Phys. Chem.*, 1993, **97**, 12020–12026.
7 D. F. A. Koch, D. A. N. Rand and R. Woods, *J. Electroanal. Chem.*, 1976, **70**, 73–78.
8 N. R. Elezovi, B. M. Babi, V. R. Radmilovi, S. L. Gojkovic, N. V. Krstajic and M. L. Vracar, *J. Power Sources*, 2008, **175**, 250–256.
9 Y. Y. Feng, L. B. Xiao, Z. H. Liu, D. S. Kong and Z. Y. Yu, *J. Catal.*, 2012, **290**, 18–25.
10 K. B. Zhou and Y. D. Li, *Angew. Chem., Int. Ed.*, 2012, **51**, 602–613.
11 D. S. Wang and Y. D. Li, *Adv. Mater.*, 2011, **23**, 1044–1060.
12 B. Lim, M. J. Jiang, P. H. C. Camargo, E. C. Cho, J. Tao, X. M. Lu, Y. M. Zhu and Y. N. Xia, *Science*, 2009, **324**, 1302–1305.
13 L. X. Ding, A. L. Wang, G. R. Li, Z. Q. Liu, W. X. Zhao, C. Y. Su and Y. X. Tong, *J. Am. Chem. Soc.*, 2012, **134**, 5730–5733.
14 M. Oezaslan, M. Heggen and P. Strasser, *J. Am. Chem. Soc.*, 2012, **134**, 514–524.
15 X. M. Ma, H. Meng, M. Cai and P. K. Shen, *J. Am. Chem. Soc.*, 2012, **134**, 1954–1957.
16 V. R. Stamenkovic, B. Fowler, B. S. Mun, G. F. Wang, P. N. Ross, C. A. Lucas and N. M. Markovic, *Science*, 2007, **315**, 493–497.
17 C. K. Poh, Z. Q. Tian, J. J. Gao, Z. L. Liu, J. Y. Lin, Y. P. Feng and F. B. Su, *J. Mater. Chem.*, 2012, **22**, 13643.
18 M. J. S. Farias, W. Cheuquepán, A. A. Tanaka and J. M. Feliu, *ACS Catal.*, 2017, **7**, 3434–3445.
19 C. Cui, L. Gan, M. Heggen, S. Rudi and P. Strasser, *Nat. Mater.*, 2013, **12**, 765–771.
20 C. Wang, N. M. Markovic and V. R. Stamenkovic, *ACS Catal.*, 2012, **2**, 891–898.
21 J. C. C. Gómez, R. Moliner and M. J. Lázaro, *Catalysts*, 2016, **6**, 130.
22 A. S. Moura, J. L. C. Fajín, M. Mandado and M. N. D. S. Cordeiro, *Catalysts*, 2017, **7**, 47.
23 L. L. Feng, G. Gao, P. Huang, X. S. Wang, C. L. Zhang, J. L. Zhang, S. W. Guo and D. X. Cui, *Nanoscale Res. Lett.*, 2011, **6**, 551.
24 N. M. Markovic and P. N. Ross, *Surf. Sci. Rep.*, 2002, **45**, 121–124.
25 F. J. Vidal-Iglesias, R. M. Arán-Ais, J. Solla-Gullón, E. Garnier, E. Herrero, A. Aldaz and J. M. Feliu, *Phys. Chem. Chem. Phys.*, 2012, **14**, 10258–10265.
26 Y. Z. Lu, Y. Y. Jiang, H. Wu and W. Chen, *J. Phys. Chem. C*, 2013, **117**, 2926–2938.

27 Z. L. Liu, X. H. Zhang and L. Hong, *Electrochem. Commun.*, 2009, **11**, 925–928.
28 X. Zhao, J. Zhang, L. J. Wang, H. X. Li, Z. L. Liu and W. Chen, *ACS Appl. Mater. Interfaces*, 2015, **7**, 26333–26339.
29 Y. C. Yan, H. Shan, G. Li, F. Xiao, Y. Y. Jiang, Y. Y. Yan, C. H. Jin, H. Zhang, J. B. Wu and D. Yang, *Nano Lett.*, 2016, **16**, 7999–8004.
30 F. W. Zhan, T. Bian, W. Zhao, H. Zhang, M. S. Jin and D. Yanga, *CrystEngComm*, 2014, **16**, 2411–2416.
31 Y. L. Qin, Y. C. Liu, F. Liang and L. M. Wang, *ChemSusChem*, 2015, **8**, 260–263.
32 Y. Zhang, X. Zhu, J. Guo and X. Q. Huang, *ACS Appl. Mater. Interfaces*, 2016, **8**, 20642–20649.
33 L. R. Nan, Z. T. Fan, W. B. Yue, Q. Dong, L. S. Zhu, L. Yang and L. Z. Fan, *J. Mater. Chem. A*, 2016, **4**, 8898–8904.
34 M. Wang, Z. Z. Ma, R. X. Lia, B. Tang, X. Q. Bao, Z. H. Zhang and X. G. Wang, *Electrochim. Acta*, 2017, **227**, 330–344.
35 P. Wu, Y. Y. Huang, L. T. Kang, M. X. Wu and Y. B. Wang, *Sci. Rep.*, 2015, **5**, 14173.
36 D. T. Phan and G. S. Chung, *Sens. Actuators, B*, 2014, **199**, 354–360.
37 W. X. Niu, Z. Y. Li, L. H. Shi, X. Q. Liu, H. J. Li, S. Han, J. Chen and G. B. Xu, *Cryst. Growth Des.*, 2008, **8**, 4440–4444.
38 W. X. Niu, L. Zhangand and G. B. Xu, *ACS Nano*, 2010, **4**, 1987–1996.
39 Q. Yuan, Z. Zhou, J. Zhuanga and X. Wang, *Chem. Commun.*, 2010, **46**, 1491–1493.
40 V. Di Noto, E. Negro, R. Gliubizzi, S. Lavina, G. Pace, S. Gross and C. Maccato, *Adv. Funct. Mater.*, 2007, **17**, 3626–3638.
41 H. A. Gasteiger and N. M. Marković, *Science*, 2009, **324**, 48–49.
42 M. P. Mercer, D. Plana, D. J. Fermín, D. Morgan and N. Vasiljevic, *Langmuir*, 2015, **31**, 10904–10912.
43 A. Vaskevich and E. Gileadi, *J. Electroanal. Chem.*, 1998, **442**, 147–150.
44 B. K. Lim, M. J. Jiang, P. H. C. Camargo, E. C. Cho, J. Tao, X. M. Lu, Y. M. Zhu and Y. Xia, *Science*, 2009, **324**, 1302–1305.
45 X. Cao, N. Wang, Y. Han, C. Z. Gao, Y. Xu, M. X. Li and Y. H. Shao, *Nano Energy*, 2015, **12**, 105–114.
46 G. Xueqing, L. Fumin, L. Yumei, L. Shuni, Y. Chen and L. Jong-Min, *J. Power Sources*, 2015, **280**, 491–498.
47 S. Yang, C. Shen, Y. Tian, X. Zhang and H. J. Gao, *Nanoscale*, 2014, **6**, 13154–13162.
48 O. Winjobi, Z. Y. Zhang, C. H. Liang and W. Z. Li, *Electrochim. Acta*, 2010, **55**, 4217–4221.
49 C. G. Hu, Z. Y. Bai, L. Yang, J. Lv, K. Wang, Y. M. Guo, Y. X. Cao and J. G. Zhou, *Electrochim. Acta*, 2010, **55**, 6036–6041.
50 S. H. Aboutalebi, A. T. Chidembo, M. Salari, K. Konstantinov, D. Wexler, H. K. Liu and S. X. Dou, *Energy Environ. Sci.*, 2011, **4**, 1855–1865.
51 A. Brouzgoua, S. Q. Song and P. Tsiakaras, *Appl. Catal., B*, 2012, **127**, 371–388.
52 I. M. Hsing, X. Wang and Y. J. Leng, *J. Electrochem. Soc.*, 2011, **149**, A615.
53 G. Wu, L. Li and B. Q. Xu, *Electrochim. Acta*, 2004, **50**, 1.
54 I. Danaee, M. Jafarian, F. Forouzandeh, F. Gobal and M. G. Mahjani, *Int. J. Hydrogen Energy*, 2009, **34**, 859–869.
55 D. Hao, X. Z. Shi, C. M. Shen, H. Chao, Z. C. Xu, L. Chen, T. Yuan, D. K. Wang and H. J. Gao, *Chin. Phys. B*, 2010, **19**, 106104.
56 G. X. Chen, Y. M. Tan, B. H. Wu, G. Fu and N. F. Zheng, *Chem. Commun.*, 2012, **48**, 2758–2760.
57 Q. Yuan, Z. Y. Zhou, J. Zhuang and X. Wang, *Chem. Commun.*, 2010, **46**, 1491–1493.
58 B. C. Du, S. A. Rabb, C. Zangmeister and Y. Y. Tong, *Phys. Chem. Chem. Phys.*, 2009, **11**, 8231–8239.
59 M. Wang, D. J. Guo and H. L. Li, *J. Solid State Electrochem.*, 2005, **178**, 1996–2000.
60 J. S. Rebello, P. V. Samant, J. L. Figueiredo and J. B. Fernandes, *J. Power Sources*, 2006, **153**, 36–40.
61 Z. B. Wang, G. P. Yin, J. Zhang, Y. C. Sun and P. F. Shi, *Electrochim. Acta*, 2006, **51**, 5691.
62 K. W. Park, J. H. Choi, B. K. Kwon, S. A. Lee, Y. E. Sung, H. Y. Ha, S. A. Hong, H. S. Kim and A. Wieckowski, *J. Phys. Chem. B*, 2002, **106**, 1869.

